Quantitative Monitoring of Adenocarcinoma Development in Rodents by Magnetic Resonance Imaging

Joel R. Garbow,[1,3] Min Wang,[2] Yian Wang,[2] Ronald A. Lubet,[4] and Ming You[2,3]

Abstract

Purpose: Accurately following the time course of tumor progression and response to therapy in animal models of cancer is key to the development of better chemopreventive and chemotherapeutic agents. The goal of this work was to monitor quantitatively the development and progression of adenocarcinoma in a time course study of mice treated with the carcinogen urethane using *in vivo* small-animal magnetic resonance imaging (MRI).

Experimental Design: Mice treated with a single dose of urethane were imaged at four time points beginning 8 months after treatment. High-resolution images of mouse lung were obtained *in vivo* using respiratory-gated MRI methods. Individual tumors were manually segmented and their volumes calculated. At the end of the study, mice were euthanized and MRI tumor quantification was validated by histology and histopathology.

Results: Tumors as small as 0.4 mm in diameter can be detected and quantitatively measured in mice by *in vivo* MRI. Total tumor burden increased consistently in all mice studied, whereas the growth rate of individual tumors varied widely. The positions and diameters of individual tumors as measured by MRI correlated well with histology results. Histologic study of large, rapidly growing tumors showed that these were adenocarcinomas, whereas small, slowly growing lesions were predominantly adenomas.

Conclusions: Longitudinal *in vivo* MRI is a powerful modality that can be of great aid in elucidating the factors that control the onset of lung tumors and can serve as a platform for the development and preclinical testing of novel therapies having a high likelihood of efficacy in human clinical trials.

Lung cancer is the leading cause of cancer death in men and women in the United States (1). Despite major advances in recent years, most lung cancers are disseminated at the time of presentation and have a mortality rate of nearly 90% (2). Revolutions in molecular biology and genomics have led to the development of many new rodent models of disease. Many of the known genetic alterations commonly found in both mouse and human lung tumors suggest that there are similarities in the development of lung cancer in rodents and humans at the molecular level (3, 4). In particular, the A/J mouse lung tumor model is similar histologically and molecularly to bronchioloalveolar carcinomas and papillary tumors, two subtypes of human adenocarcinoma, and has been widely used in studies of the genetics of lung tumors (4). In many carcinogen-treated mice, early disease is characterized by the development of small, nonmalignant adenomas, whereas malignant, highly aggressive, invasive carcinomas appear in the later stages of disease. A major outstanding challenge in lung cancer biology is to identify and distinguish adenocarcinomas that develop at the sites of early-stage adenomas from those that instead form at separate and unique sites within the lung (5, 6). Longitudinal studies of mice with developing tumors can readily distinguish between slowly and rapidly growing lesions and can help to determine whether the initial growth rates are predictive of later adenocarcinoma development. In addition, such studies may help identify early lesions that, because of a rapid growth rate or location within the lung, will become adenocarcinomas despite a relatively small size at detection.

Magnetic resonance imaging (MRI) is a powerful imaging modality for characterizing animal systems and animal models of disease. As a noninvasive, nondestructive technique, *in vivo* MRI permits a wide variety of longitudinal studies not possible with other destructive analytic methods. Whereas the opportunities for characterization are significant, lungs present unique challenges for MRI, requiring the development of new and innovative methods (7–9). A review of small-animal MRI of lungs has recently appeared (10). The study of normal lung tissue by ^{1}H magnetic resonance methods presents challenges different from most other tissues: (*a*) Low tissue density and low water content within the lung severely limit signal-to-noise. (*b*) Variations in magnetic susceptibility associated with the

Authors' Affiliations: Departments of [1]Radiology and [2]Surgery and [3]The Alvin J. Siteman Cancer Center, Washington University School of Medicine, St. Louis, Missouri; and [4]Division of Cancer Prevention, National Cancer Institute, Bethesda, Maryland

Received 7/17/07; revised 11/19/07; accepted 12/13/07.

Grant support: NIH/National Cancer Institute Small Animal Imaging Resource Program grant R24 CA83060, NIH/National Cancer Institute Molecular Genetics of Mouse Lung Tumors grant R01 CA58554, the Alvin J. Siteman Cancer Center at Washington University in St. Louis, a National Cancer Institute Comprehensive Cancer Center grant P30 CA91842.

The costs of publication of this article were defrayed in part by the payment of page charges. This article must therefore be hereby marked *advertisement* in accordance with 18 U.S.C. Section 1734 solely to indicate this fact.

Requests for reprints: Joel R. Garbow, Biomedical MR Laboratory, Campus Box 8227, 4525 Scott Avenue, St. Louis, MO 63110. Phone: 314-362-9949; Fax: 314 362 0526; E-mail: garbow@wustl.edu.

doi:10.1158/1078-0432.CCR-07-1757

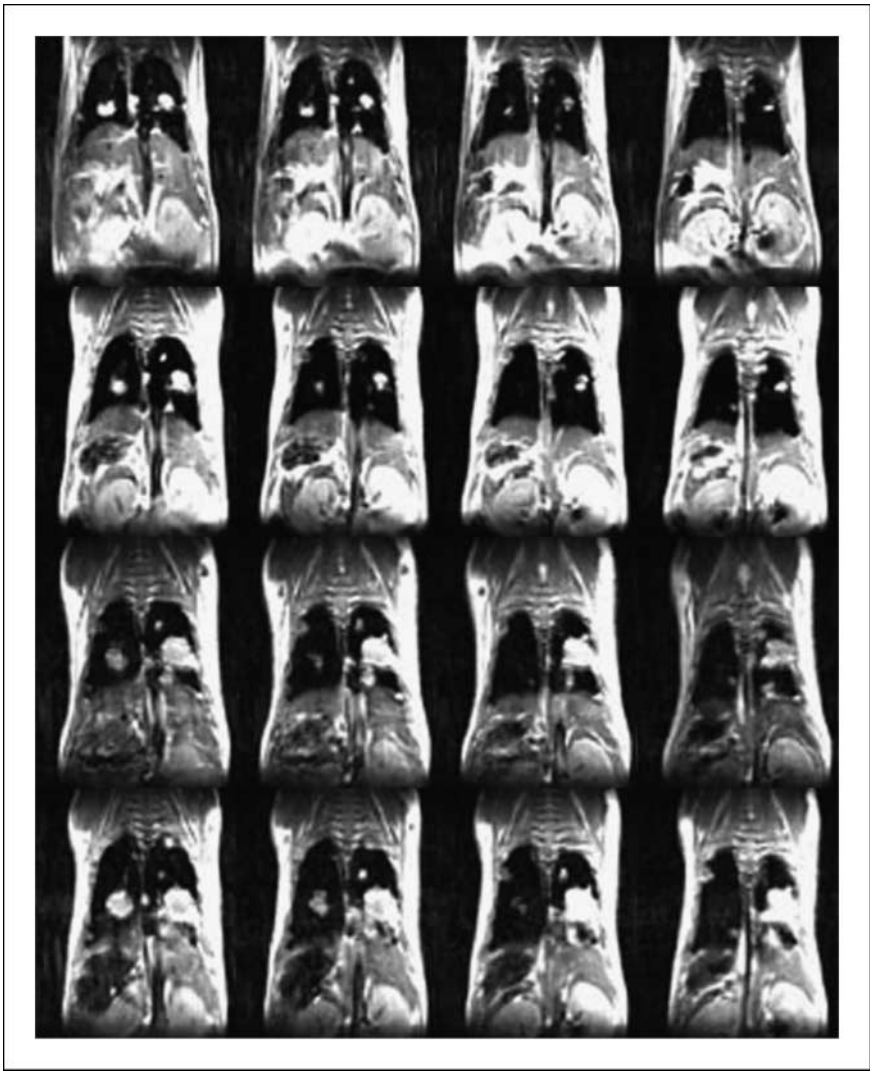

Fig. 1. Contiguous coronal slices, ventral to dorsal, from a series of respiratory-gated, spin-echo magnetic resonance images of an A/J mouse collected at four different time points ranging from 8 mo (*top row*) to 12 mo (*bottom row*) following treatment with urethane. Images were collected with repetition time, ~3 s; echo time, 20 ms; field of view, 2.5 × 2.5 cm^2; slice thickness, 0.5 mm; 128 × 128 data matrix; four averages. The time-course progression of disease can be clearly seen in these images.

many air-tissue interfaces of the alveoli and bronchioles result in short T2* and T2 relaxation times, thus further contributing to low signal-to-noise. (*c*) Respiratory and cardiac motions lead to significant image blurring in the absence of motion-synchronized data acquisition.

Previously, we have shown that respiratory-gated ^{1}H MRI can reliably detect submillimeter lung lesions *in vivo* in mice (11). In this study, we extend this earlier work to provide detailed, quantitative characterization of the progression of adenocarcinoma in a longitudinal study of mice treated with the carcinogen urethane. The time to development of individual tumors within the mouse lung is reliably and quantitatively measured. MRI results are validated with conventional histopathologic measures. The thus shown ability to noninvasively detect lung tumors at an early stage of disease and follow their progression longitudinally enables a wide variety of studies that provide insight into the factors influencing the onset and progression of lung cancer. Mouse models of human cancers afford unique opportunities to evaluate novel therapies in preclinical trials. This study also serves to establish MRI characterization of tumors in murine models of lung cancer as a potential preclinical benchmark for evaluating novel chemopreventive and chemotherapeutic agents having a high likelihood of efficacy in human clinical trials.

Materials and Methods

Reagents and animals. For mouse lung tumor bioassays, A/J male mice at 4 weeks of age were purchased from The Jackson Laboratory. Urethane was purchased from Sigma Chemical Co. Mice were housed in plastic cages with hardwood bedding and dust covers in a HEPA-filtered, environmentally controlled room (24 ± 1°C, 12:12 h light/dark cycle) and were given Rodent Lab Chow, #5001 (Purina), and water *ad libitum*. When the animals reached 6 weeks of age, lung tumor bioassay was initiated by a single i.p. injection of urethane (1 mg/g body weight) in 0.2-mL PBS. Mice were imaged 8 months after the initial dose of urethane (imaging day 0) and subsequently on days 32, 102, and 116. Immediately following the last imaging point (11.5 months after initial treatment), all animals were euthanized by CO_2 asphyxiation. Lungs from each mouse were inflated and fixed in Tellyesniczky's solution for 18 to 24 h and then transferred to 70% alcohol. Paraffin embedding and H&E staining were done on selected mouse lung tumors following routine procedures.

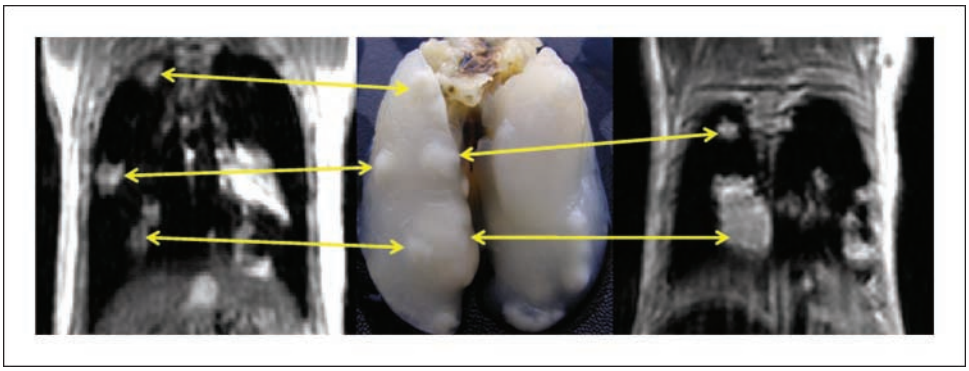

Fig. 2. Two slices from a series of coronal, respiratory-gated, spin-echo images of urethane-treated A/J mouse (*left*, *right*), together with a photograph of the lungs from this mouse, harvested immediately following the collection of these images. Yellow arrows, one-to-one correspondence between tumors in the image and those observed in the photograph.

MRI. Respiratory-gated, spin-echo magnetic resonance images of mice were collected with a small-animal magnetic resonance scanner based on an Oxford Instruments 4.7-T, 40-cm bore magnet. The magnet is equipped with Magnex Scientific actively shielded, high-performance (10 cm ID, ~50 G/cm, ~200 μs rise-time) gradient coils and Techron gradient power supplies and is interfaced with a Varian NMR Systems INOVA console. All data were collected using a Stark Contrast 2.5-cm birdcage-style rf coil. Before the imaging experiments, mice were anesthetized with isoflurane and were maintained on isoflurane/O_2 (1-1.25%, v/v) throughout data collection. Animal core body temperature was maintained at 37 ± 1°C by circulation of warm air through the bore of the magnet. During the imaging experiments, the respiration rates for all mice were regular and ~2 s^{-1}. Synchronization of magnetic resonance data collection with animal respiration was achieved with a home-built respiratory-gating unit (12) and all images were collected during post-expiratory periods. Twenty-four to thirty contiguous coronal slices, ventral to dorsal, were collected for each mouse. Imaging parameters were repetition time, ~3 s; echo time, 20 ms; field of view, 2.5 × 2.5 cm^2; slice thickness, 0.5 mm; 128 × 128 data matrix; four averages.

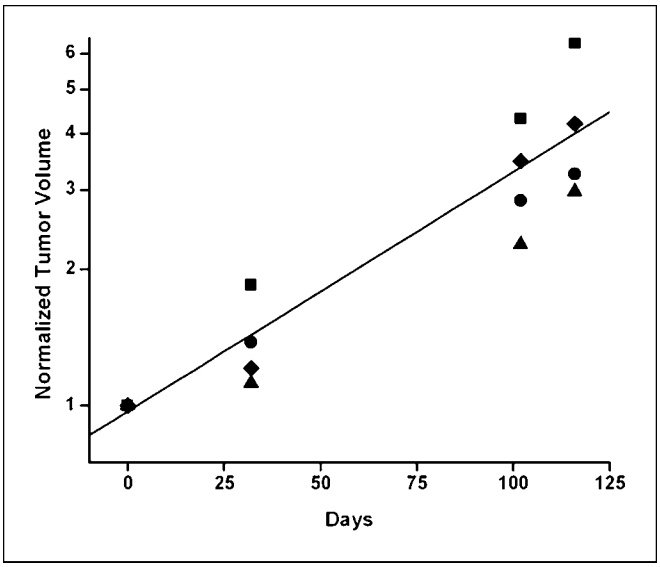

Fig. 3. Growth curves showing total tumor burden as a function of time for four A/J mice following treatment with urethane. The first set of images was collected ~6 mo following the urethane treatment (day 0 images); subsequent images were collected 32, 102, and 116 d later. For each animal, tumor burdens are normalized to their day 0 values; actual total tumor volumes at day 0 ranged from 0.86 to 1.87 mm^3. Data are plotted in semi-log format to emphasize the exponential nature of tumor growth; the straight line is the semi-log linear regression through all of the data points.

Lung tumor volume calculations. As in our previous studies (11), we found that coronal images were the most useful for visualizing lung tumors and measuring their volumes. Multislice coronal images were collected that spanned the entire mouse, ensuring complete coverage of the lungs. Regions of interest were manually drawn around tumors in each slice of the multislice images using either Varian's Image Browser software or NIH ImageJ[5] software and volumes of the resulting segmented regions were calculated. Consistent results were achieved using either Image Browser or ImageJ. Tumor volumes were calculated for each segmented region of interest; volumes from contiguous regions of interest in adjacent slices were grouped together to yield individual tumor volumes.

Results and Discussion

As described in Introduction, normal lung tissues present several unique challenges to study by MRI. However, as we have recently shown (11), the very factors that make it difficult to image healthy lung parenchyma, including low tissue density, low water content, and variations in magnetic susceptibility within the lung, aid in the detection of tumors by increasing the contrast between healthy and pathologic tissue. Figure 1 shows a longitudinal series of four contiguous coronal, respiratory-gated spin-echo images, ventral to dorsal, of an A/J mouse, collected at four different time points ranging from 8 to 12 months following treatment with the carcinogen urethane. Images from different time points were aligned carefully by reference to the outline of the lungs and the location of other organs (e.g., heart, liver, and kidneys) visible in the images, ensuring that individual tumors can be identified and followed over time. The slices in Fig. 1 were chosen to display consistent anatomy at each time point. Within the outline of the lung in these images, tumors appear bright, whereas healthy lung tissue appears black. Progression of the lung tumors over the course of the 3.5-month study can be clearly seen in these images. A similar time-course progression of disease is seen for the other animals in this study.

Figure 2 shows an expanded view of two images from the 116-day imaging point, together with a photograph of the lungs following removal from the animal. The one-to-one correspondence of several tumors in these images and in the photograph are noted in this figure with yellow arrows; other tumors in the photograph can be clearly matched with tumors observed in other image slices.

[5] http://rsb.info.nih.gov/ij

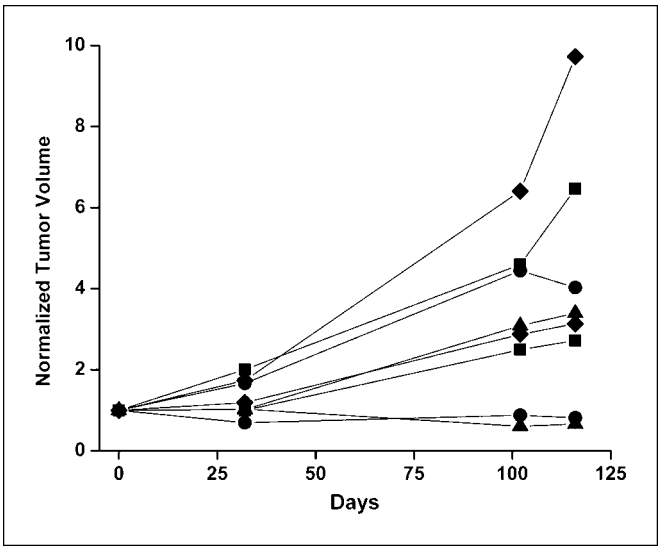

Fig. 4. Growth curves showing individual tumor growth for eight different tumors in two different A/J following treatment with urethane. Lines connecting the data points on this graph serve to guide the eye. The figure illustrates the wide variation in growth of individual tumors within the lungs.

To characterize tumor progression more quantitatively, we manually segmented the tumors in each slice of a multislice image. Figure 3 shows a graph of normalized tumor burden, plotted as a function of time on a per animal basis, for each of the four mice in this study. For each animal, *total* tumor volume at each time point was normalized to its day 0 value; actual total tumor volumes at day 0 ranged from 0.86 to 1.87 mm^3. The graph is displayed in semi-log form to emphasize the exponential nature of the tumor growth in these mice. Although there is some animal-to-animal variation, the tumor growth curves from these four mice are quite similar, and the measured tumor burdens agree well with those estimated by histology.

Whereas the total tumor growth curves for each of the four mice are similar, there is considerable variation in the growth of individual tumors within each animal. Figure 4 shows the growth curves for eight individual tumors measured in two different animals. Lines connecting the data points on this graph serve to guide the eye. For each individual tumor, all measured volumes were normalized to the day 0 value of that tumor. As illustrated in Fig. 4, the volumes of aggressive tumors can increase by nearly an order of magnitude (10×) over a period of 116 days. By contrast, other lesions only double in size over this same time period, and some grow very little or even shrink modestly in size. Major tumor-to-tumor growth variations seen within each animal emphasize the importance of characterizing tumor growth and development with a technique like MRI that can visualize and measure individual tumor volumes. Monitoring lesion development and correlating this development with histopathology are keys to developing insight into the factors influencing the onset and progression of lung cancer. Similar considerations hold for chemotherapy and chemoprevention studies, in which the ability to monitor therapeutic response for individual lesions will enhance our understanding of the factors that contribute to positive response.

A subset of the tumors found in the lungs of these mice was submitted for detailed histologic analysis. Figure 5 shows representative H&E stains of normal lung parenchyma (*left*), adenoma (*middle*), and adenocarcinoma (*right*) in a lung harvested from a urethane-treated mouse. Consistent with previously published results correlating lesion size with tumor progression (11, 13), the H&E stain in the center panel is of tissue from a small (~0.5 mm diameter) lesion, whereas the stain in the right panel is of tissue from a large (>2-mm diameter) lesion. Adenocarcinoma is characterized by multiple well-defined focal lesions, frequently situated just below the visceral pleura, which increase in both size and number as disease progresses. As we previously reported (11), histologically, lung adenocarcinomas often display a highly infiltrative character, with marked cellular atypia and pleomorphism. Features of lung adenoma cells include a papillary pattern and some compression of adjacent parenchyma, consisting of monomorphic, generally well-differentiated cells supported by fibrovascular stroma. In this study, histologic examination reveals the tumors to be mixtures of adenoma and adenocarcinoma.

The results from this quantitative MRI analysis of individual lung tumors (Fig. 4) correlate well with the reported histopathology of these tumors. Histologically, tumors growing

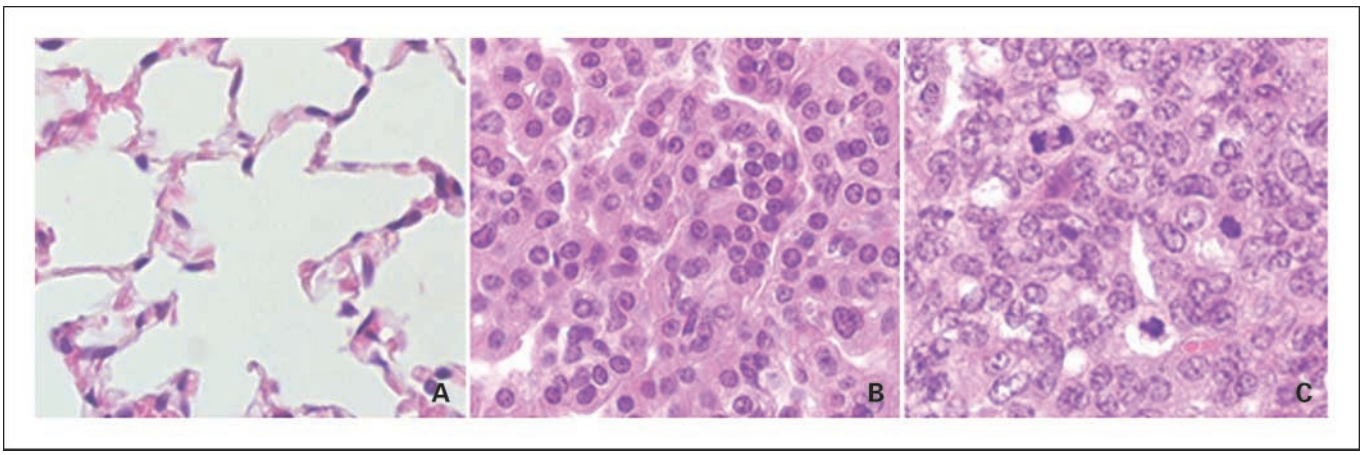

Fig. 5. H&E stains of lung tissue (400× amplification) isolated from urethane-treated mice: normal lung parenchyma (*left, A*), adenoma (*middle, B*), and adenocarcinoma (*right, C*). Middle, the H&E stain is of tissue from a lesion that is ~0.5 mm in diameter; right, the stain is of tissue from a lesion >2 mm in diameter.

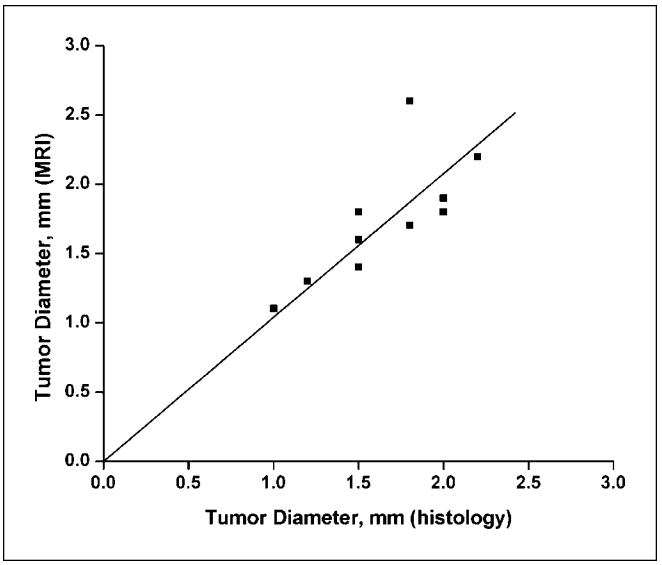

Fig. 6. Scatter plot of tumor diameters measured by histology and MRI, showing the strong positive correlation between these measurements. The straight line shown on this plot is a least squares fit of the data points, with the constraint that the line passes through the data point (0, 0). The slope of this line is 1.03 and the correlation coefficient (r) is 0.71.

most quickly, as determined by MRI, are adenocarcinomas whereas tumors growing most slowly are predominantly adenomas. In addition, tumors measured by MRI can also be correlated, in both size and position, with the results of conventional histology experiments. We have established a one-to-one correspondence between tumors detected by *in vivo* magnetic resonance and those observed *ex vivo* following harvesting of the lungs. Figure 6, a scatter plot presentation of tumor diameters measured by magnetic resonance and histology, shows that these tumor diameters are highly correlated. The straight line shown on this plot is a least squares fit of the data points, with the constraint that the line passes through the data point (0, 0). The slope of this line is 1.03 and the correlation coefficient (r) is 0.71, showing the excellent agreement in *absolute* tumor size as measured by MRI and histology. Tumors as small as 0.4 mm in diameter can be detected and measured quantitatively *in vivo* by MRI and correlated with specific tumors in the mouse lung.

The results presented in this article show that MRI is a powerful imaging modality for the *in vivo* characterization of lung tumors in mice. The data clearly show that MRI can detect submillimeter tumors in mouse lung and that the size and growth properties of these tumors correlate well with histologic and histopathologic data. Because MRI is noninvasive and nondestructive and uses nonionizing radiation, it is an ideal method for longitudinal studies of tumor development and therapeutic response. With the wide array of transgenic mice that are now available, we are confident that MRI will provide important insights into the factors that control the onset and development of tumors and will serve as an important platform for the preclinical development and evaluation of novel chemopreventive and chemotherapeutic agents having a high likelihood of efficacy in human clinical trials.

Acknowledgments

We thank John Engelbach for help with data processing and analysis.

References

1. Minna J, Roth J, Gazdar A. Focus on lung cancer. Cancer Cell 2002;1:49–52.
2. Greenlee RT, Murray T, Bolden S, Wingo PA. Cancer statistics. CA Cancer J Clin 2000;50:7–33.
3. Herzog CR, Lubet RA, You M. Genetic epigenetic alterations in mouse lung tumors: implications for cancer chemoprevention. J Cell Biochem 1997;28/29S: 49–63.
4. Minna JD. The molecular biology of lung cancer pathogenesis. Chest 1993;103:449–56.
5. Foley J, Anderson M, Stoner G, Gaul B, Hardisty J, Maronpot R. Proliferative lesions of the mouse lung: progression studies in strain A mice. Exp Lung Res 1991;17:157–68.
6. Shimkin M, Stoner G. Lung tumors in mice: application to carcinogenesis bioassay. Adv Cancer Res 1975;21:1–58.
7. Hedlund L, Dewalt S, Cofer G, Johnson GA. MR microscopy of the lung. In: Cutillo A, editor. Application of magnetic resonance to the study of the lung. Armonk, New York: Futura Press; 1996. p. 401–15.
8. Dugas J, Garbow J, Kobayashi D, Conradi M. Hyperpolarized 3He MRI of mouse lung. Magn Reson Med 2004;52:1310–7.
9. Huang M, Basse P, Yang Q, Horner J, Hichens T, Ho C. MRI detection of tumor in mouse lung using partial liquid ventilation with a perfluorocarbon-in-water emulsion. Magn Reson Imaging 2004;22: 645–52.
10. Schuster DP, Kovacs A, Garbow J, Piwnica-Worms D. Recent advances in imaging the lungs of intact small animals. Am J Respir Cell Mol Biol 2004;30: 129–38.
11. Garbow JR, Zhang Z, You M. Detection of primary lung tumors in rodents by magnetic resonance imaging. Cancer Res 2004;64:2740–2.
12. Garbow J, Dugas J, Song S-K, Conradi M. A simple, robust hardware device for passive or active respiratory gating in MRI and MRS experiments. Concepts Magn Reson B Magn Reson Eng 2004; 21B:40–8.
13. Zhang Z, Wang Y, Yao R, et al. Cancer chemopreventive activity of a mixture of Chinese herbs (antitumor B) in mouse lung tumor models. Oncogene 2004;23: 3841–50.

Clinical Cancer Research

Quantitative Monitoring of Adenocarcinoma Development in Rodents by Magnetic Resonance Imaging

Joel R. Garbow, Min Wang, Yian Wang, et al.

Clin Cancer Res 2008;14:1363-1367.